Mineral Kaolinite Clay for Preparation of Nanocomposite Hydrogels

M. Sirousazar,[1] M. Kokabi,[1] Z. M. Hassan,[2] A. R. Bahramian[1]

[1]*Polymer Engineering Department, Faculty of Chemical Engineering, Tarbiat Modares University, Tehran, I.R. Iran*
[2]*Immunology Department, Faculty of Medical Sciences, Tarbiat Modares University, Tehran, I.R. Iran*

Received 10 May 2011; accepted 14 June 2011
DOI 10.1002/app.35095
Published online 28 December 2011 in Wiley Online Library (wileyonlinelibrary.com).

ABSTRACT: In this work, nanocomposite hydrogels on the basis of polyvinyl alcohol and mineral kaolinite clay were prepared via freezing–thawing cyclic method without using any chemical crosslinkers as well as any intercalants for modification of kaolinite. The nanocomposite hydrogels were characterized by XRD, TEM, SEM, and FTIR methods. The effect of kaolinite content on the gel fraction values of nanocomposite hydrogels was investigated. Thermal and mechanical properties of prepared nanocomposite hydrogels were also studied using the DSC, DMTA, and hardness tests. Finally, the swelling and dehydration kinetics of nanocomposite hydrogels were studied at different temperatures. The morphology of prepared nanocomposite hydrogels was determined as intercalated morphology on the basis of XRD and TEM techniques. The role of kaolinite in the creation of supramolecular crosslinked network of polyvinyl alcohol was exhibited by FTIR and gel fraction tests. The thermal and mechanical experiments showed the reinforcing effect of kaolinite in the polyvinyl alcohol matrix. Swelling and dehydration tests showed that an increase of kaolinite content causes a decrease in the swelling ratio as well as in the dehydration rate of nanocomposite hydrogels. On the other hand, direct dependences of the swelling ratio and dehydration rate to the temperature were observed for all nanocomposite hydrogels. © 2011 Wiley Periodicals, Inc. J Appl Polym Sci 125: E122–E130, 2012

Key words: nanocomposites; hydrogels; clay

INTRODUCTION

Polyvinyl alcohol (PVA) is a synthetic hydrogel which due to its good chemical and mechanical stability, processability, biocompatibility, and biodegradability has been used in numerous biomedical applications such as implant,[1] artificial organ,[2] contact lens,[3] drug delivery device,[4,5] and also wound dressing.[6–8] PVA hydrogel is prepared by crosslinking the linear chains of PVA. There are different methods for preparation of PVA hydrogel such as electron beam irradiation, chemical crosslinking using crosslinking agents such as formaldehyde and glutaraldehyde, and also freezing–thawing cyclic process.[9] Among these methods, the freezing–thawing technique has a remarkable advantage of crosslinking the PVA polymer solution without leaving any crosslink remnant in the hydrogel matrix.[10–12] Thus, the freeze-thawed PVA hydrogel as a promising material can be used in a wide range of biomedical applications.

In recent years, several attempts have been made to reinforce the structure of polymeric hydrogels by incorporating the nanoparticles or nanostructures to obtain the nanocomposite hydrogels with improved mechanical, physical, and chemical properties.[13] Nanocomposite hydrogels are reinforced three-dimensional networks consisting of at least a crosslinked polymeric matrix and a nanometric reinforcing agent, such as clay silicate layers.[14] Nanocomposite hydrogels have been utilized successfully in numerous practical applications such as sensor and actuator systems,[15] oil recovery,[16] biomedical scaffolds,[17] drug-delivery devices,[18,19] and wound-dressing systems.[20,21] The most attentions on the polymer–clay nanocomposite hydrogels have been focused on the use of laponite,[22] montmorillonite,[23,24] and hydrotalcite[25] as reinforcing agents.

Kaolinite with ideal composition of $Al_2Si_2O_5(OH)_4$ is a 1 : 1 dioctahedral clay having widespread applications in the manufacture of paper, ceramics, inks and paints, and also as adsorbent in pollution control processes and water treatments.[26,27] In addition, it has been used as a filler in production of rubber and polymer-based composite and nanocomposite materials.[27–30] Nonetheless, it has not been utilized in production of nanocomposite hydrogels and only a few studies are available on the kaolinite based composite hydrogels.[31–34]

Correspondence to: M. Kokabi (mehrir@modares.ac.ir).
Contract grant sponsors: Tarbiat Modares University and Iran Nanotechnology Initiative Council (INIC).

To increase the interlayer space of kaolinite, some intercalants such as dimethyl sulfoxide (DMSO) or potassium acetate are used.[35] Although these intercalants create good conditions for preparation of nanocomposite hydrogels with better intercalation of polymer chains in basal spacing of clay, but in general these compounds are toxic and the resulting modified clay is not proper for biomedical and food applications, particularly when the modified clay content in polymer matrix is high.[36]

In this work, a novel series of supramolecular polymer–clay nanocomposite hydrogels on the basis of PVA and kaolinite were prepared without using any additional crosslinker or intercalant compounds. It seems that the prepared nanocomposite hydrogels could be good candidates for biomedical applications. The PVA/kaolinite nanocomposite hydrogels were prepared via the cyclic freezing–thawing technique and their morphological, structural, thermal, and mechanical properties were studied. The swelling and dehydration mechanisms of prepared nanocomposite hydrogels were also investigated.

EXPERIMENTAL

Materials

PVA having a degree of saponification of greater than 98% and average number of molecular weight of 74800 was purchased from Nippon Gohsei, Japan. Pharmaceutical grade of Kaolinite (Kaolin Powder) was purchased from Merck, Darmstadt, Germany and used as received without further purification or modification. Double distilled water (DDW) was used in the preparation of all aqueous solutions.

Preparation of nanocomposite hydrogels

To prepare each nanocomposite hydrogel, an adequate amount of kaolinite powder was added to DDW and mixed to achieve a kaolinite suspension. PVA was gradually added to the kaolinite suspension and mixed for 4 h at 90°C to achieve complete dissolution. All prepared solutions had 15 wt % of PVA (based on the total mass of solution) and 0, 5, 10, and 15 wt % of kaolinite (based on the mass of PVA and kaolinite). The solutions then poured in plastic molds and placed at −20°C for 24 h to induce crystallization and gel formation. After the freezing process, they were subsequently allowed to thaw for 24 h at room temperature. The freezing–thawing cycles were repeated three times for each solution. Finally, the prepared freeze-thawed hydrogels were kept in their molds until further experiments were performed. The designations and detailed compositions of the prepared samples have been listed in Table I.

TABLE I
Designations and Chemical Compositions of Prepared Hydrogels

Sample designation	PVA (wt %)	Kaolinite (wt %)	Water (wt %)	$\frac{\text{Kaolinite} \times 100}{\text{PVA} + \text{Kaolinite}}$
PVA	15	0	85	0
PVA/5 wt % Kaolinite	15	0.79	84.21	5
PVA/10 wt % Kaolinite	15	1.67	83.33	10
PVA/15 wt % Kaolinite	15	2.65	82.35	15

Characterization

X-ray diffractometry (XRD) was used to determine the morphology of nanocomposite hydrogels. All examined samples including the kaolinite powder and nanocomposite hydrogels were dried in a vacuum oven for at least 48 h and then characterized using a Philips diffractometer at a scanning rate of 2°/min. The microstructure of nanocomposite hydrogel containing 5 wt % kaolinite was also observed using transmission electron microscopy (TEM). First, the sample was completely dried under vacuum and then embedded in an epoxy matrix. Subsequently, it was cut to 70–100 nm thick section with a diamond knife and placed onto a 400-mesh copper grid. Observation was performed using a Philips electron microscope (EM 208 S) with an acceleration voltage of 100 kV. Scanning electron microscopy (SEM) was used to observe the surface morphological aspects of the prepared nanocomposite hydrogels. Hydrogels containing 0, 5, and 15 wt % of kaolinite were frozen in liquid nitrogen and then freeze-dried at −40°C for 12 h. Subsequently, each sample was fractured and the cross-section was coated with a thin layer of gold. The observations were carried out using a Philips XL-30 scanning electron microscope at 16 kV. The characteristic functional groups of the kaolinite, pure PVA hydrogel and nanocomposite hydrogel loaded with 5 wt % of kaolinite were analyzed by Fourier transform infrared spectrometry (FTIR) using a Thermo Nicolet (FTIR NEXUS-670) spectroscope. Each sample was completely dried under vacuum for 48 h and then grounded with dried potassium bromide (KBr) powder and compressed into a disc. Spectra were collected in the range 400–4000 cm^{-1} with 2 cm^{-1} spectral resolution and 20 scans were performed for each sample.

Gel fraction

Gel fraction test was performed by extracting uncrosslinked polymer chains from hydrogels. Preweighed slice of each hydrogel was dried under vacuum until observing no change in its mass. Nearly identical weight of another slice of the same sample

was immersed into excess amount of DDW for a week to extract uncrosslinked species. Subsequently, the immersed hydrogel was removed from DDW and dried under vacuum until the dried mass showed constant weight. The gel fraction value of the hydrogels was calculated as follows:

$$\text{Gel fraction } (\%) = \frac{m_f}{m_i} \times 100 \quad (1)$$

where m_f and m_i are the mass of the dried hydrogel after and before extraction, respectively. Gel fraction test was repeated three times for each hydrogel.

Thermal and mechanical properties

Differential scanning calorimetry (DSC) was carried out on a DSC-Netzsch-200-F3 differential scanning calorimeter. The hydrogels (each of about 10–15 mg) were completely dried in vacuum oven for 48 h prior to analysis. The analysis was performed at a scan rate of 10°C/min, in the temperature range from −50 to 150°C, under continuous nitrogen atmosphere. The dynamic mechanical–thermal analysis (DMTA) was carried out using a Rheometrics DMA 242-C (Netzsch) dynamic mechanical analyzer. The disc-shaped samples with diameter of 11 mm and thickness of 5 mm were analyzed in the compression-testing mode. The scans were performed at a frequency of 1 Hz, a ramp of 5°C/min from −100 to 100°C. The hardness of hydrogels was determined by a durometer Shore A (Bareiss, Germany). The samples were prepared according to ASTM D-2240-95 with a thickness of 6 mm. The test was performed at room temperature and the data recorded 15 s after the pressing probe touched the specimen. The hardness of at least five different sections of each sample was measured and the average value was reported.

Swelling kinetics

Three identical slices of each hydrogel (each nearly 2 g) were selected and immersed in excess amount of DDW for a week to extract uncrosslinked species. Each extracted sample was then withdrawn from DDW and dried under vacuum until to reach a constant weight (m_0). Swelling kinetics of hydrogels was determined by measuring their weight increase in DDW at various time intervals. Each extracted and dried sample was immersed into 500 mL of DDW. At desired time intervals, swollen sample was removed from DDW and weighed after gentle surface wiping by absorbent paper. Swelling experiments were performed at 20, 37, and 55°C within a GTH-072TR temperature-humidity chamber (Giant Force Instrument). The swelling ratio ($q(t)$) was calculated for each sample at desired temperature as follows:

$$q(t) = \frac{m(t)}{m_0} \quad (2)$$

where $m(t)$ is the weight of swollen hydrogel at swelling time of t. The average value of $q(t)$ was calculated on the basis of three individual tests for each sample at any desired temperature.

Dehydration

The dehydration kinetics of all hydrogels was determined gravimetrically by weighing their weight loss at constant temperatures of 20, 37, and 55°C and at predetermined time intervals. The fraction of water removed from each hydrogel at time t was calculated as follows:

$$\frac{M_t}{M_\infty} = \frac{m(t) - m(0)}{m(\infty) - m(0)} \quad (3)$$

where M_t and M_∞ are the cumulative amount of water loss of the hydrogel at any time t and the total amount of removable water from the hydrogel (the initial amount of water inside the hydrogel), respectively. $m(0)$, $m(t)$, and $m(\infty)$ are the mass of hydrogel at the initial state, time t, and the final state (dried condition), respectively.

RESULTS AND DISCUSSION

Nanocomposites morphology and structure

In Figure 1, the XRD profiles and related results of kaolinite powder and nanocomposite hydrogels have been shown. A characteristic diffraction peak at 12.3° is observed for kaolinite powder which is corresponding to the d_{001}-spacing of 7.19 Å. The nanocomposite hydrogels exhibit diffraction peaks at about 11.37–11.85°, corresponding to the d_{001}-spacings between 7.43 and 7.77 Å. Observed increases in the d_{001}-spacing of kaolinite imply that there is polymer intercalation within the silicate galleries of kaolinite in nanocomposite hydrogels and reveals of intercalated morphology. For more directly identifying the morphology of nanocomposite hydrogels, the TEM image of nanocomposite hydrogel containing 5 wt % of kaolinite was taken and shown in Figure 2. The dark lines represent the silicate layers of kaolinite and the gray-white area represents the polymer matrix. This image is clearly in accordance with the XRD results and proves the intercalated morphology for PVA/kaolinite nanocomposite hydrogels. The SEM images showing the morphology of fracture surface of pure PVA hydrogel and nanocomposite hydrogels containing 5 and 15 wt %

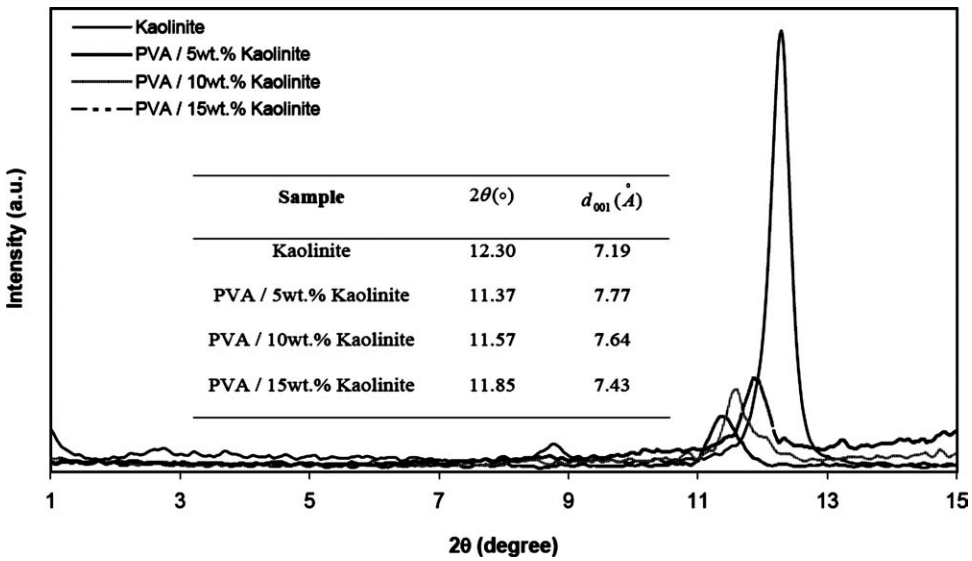

Sample	$2\theta(^\circ)$	d_{001} (Å)
Kaolinite	12.30	7.19
PVA / 5wt.% Kaolinite	11.37	7.77
PVA / 10wt.% Kaolinite	11.57	7.64
PVA / 15wt.% Kaolinite	11.85	7.43

Figure 1 XRD profiles of kaolinite powder and nanocomposite hydrogels.

of kaolinite are shown in Figure 3. A filamentous morphology with more packed structure can be observed in the fracture sections of nanocomposite hydrogels compared to the pure PVA hydrogel which could be attributed to the increase in the crystallinity of PVA chains in presence of kaolinite silicate layers.

FTIR spectrometry

Figure 4 exhibits the FTIR spectra of kaolinite, pure PVA hydrogel and nanocomposite hydrogel loaded with 5 wt % of kaolinite in the spectral scale of 4000 to 400 cm^{-1}. The typical bands of PVA hydrogel including: C—O stretching band at 1105 cm^{-1}, C—C stretching band at 1457 cm^{-1}, C—H stretching band at 2948 cm^{-1} and a broad O—H stretching band around 3220–3450 cm^{-1} are observed. The O—H stretching band of PVA hydrogel has been broaden because of crystallization of PVA chains and creation of hydrogen bonding among the hydroxyl groups of PVA during the freezing–thawing process. Figure 4 also demonstrates the characteristic bands for kaolinite at 622 and 1102 cm^{-1} attributed to the Si—O stretching bands. The band at 3710 cm^{-1} in the same spectrum is associated to the stretching vibrations of structural O—H groups at the chemical structure of the kaolinite. In the nanocomposite hydrogel, the C—O band of PVA and Si—O band of kaolinite have been overlapped and give a slightly broader band around 1114 cm^{-1}. This band confirms the presence of Si—O groups and as a result the presence of kaolinite layers in the nanocomposite hydrogel. Furthermore, the spectrum of nanocomposite hydrogel shows that the band related to the O—H groups of kaolinite has been shifted to lower wavenumbers and merged with the broad hydroxyl band of PVA, which reveals of developing some interactions between the functional O—H groups of kaolinite and PVA chains. On the basis of the FTIR results, it can be deduced that by adding kaolinite to the PVA hydrogel, some additional interactions are developed between functional groups of clay layers and hydroxyl groups on the polymer chains. The results imply the hydrogen-bonded supramolecular cross-linked networks of PVA have been created in the presence of silicate layers of kaolinite.

Gel fraction

Figure 5 shows the effect of kaolinite loading level on the gel fraction of nanocomposite hydrogels. It

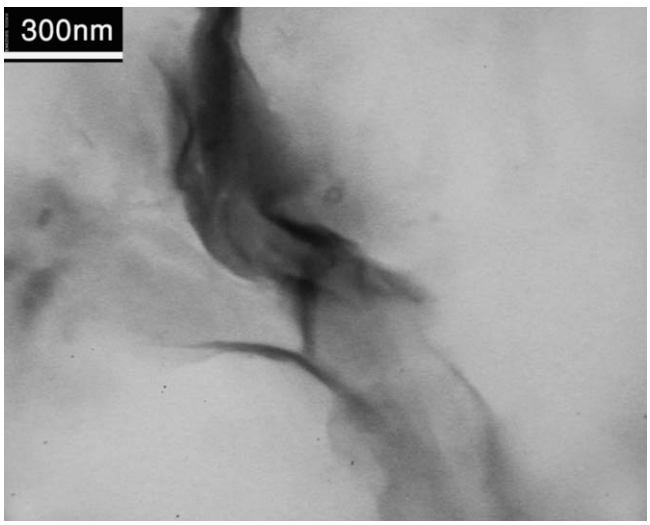

Figure 2 TEM image of nanocomposite hydrogel loaded with 5 wt % of kaolinite.

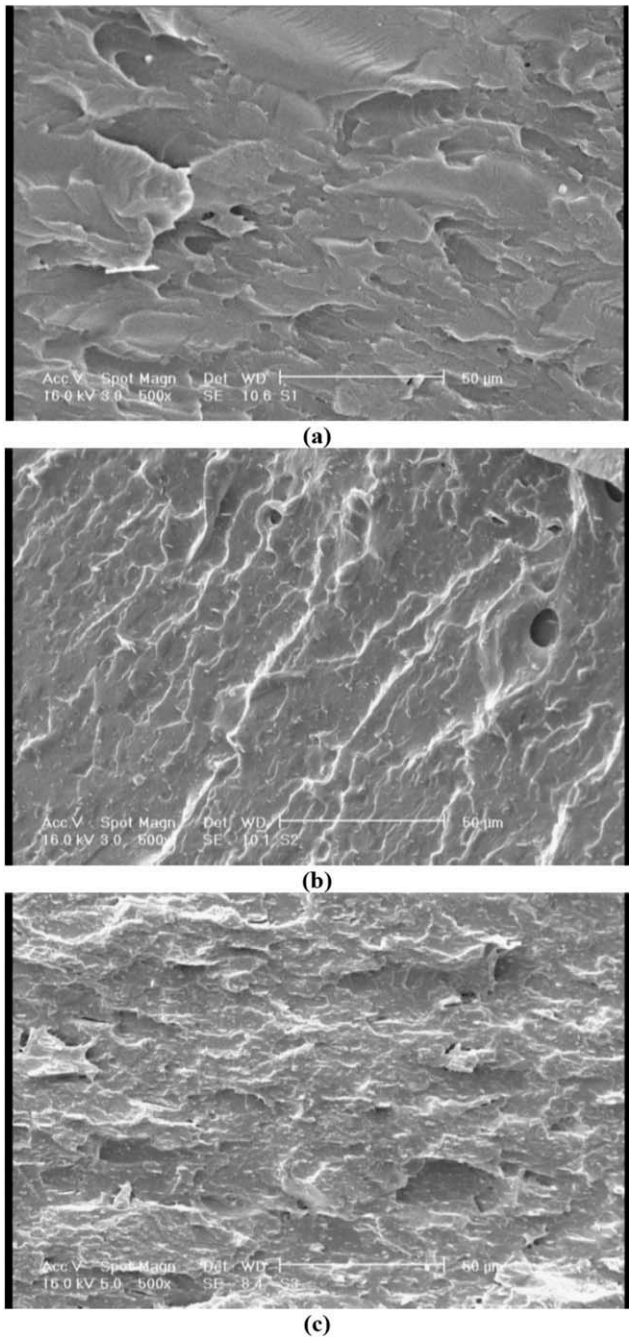

Figure 3 SEM images of (a) pure PVA hydrogel and nanocomposite hydrogels containing (b) 5, and (c) 15 wt % of kaolinite.

can be seen that the nanocomposite hydrogels have higher gel fraction values compared with the pure PVA hydrogel and the gel fraction value increases by increasing the amount of kaolinite. For instance, the gel fraction of nanocomposite hydrogel containing 15 wt % of kaolinite was enhanced by 14% as compared with the pure PVA hydrogel. This infers the development of interactions between the kaolinite layers and PVA chains and confirms the hydrogen-bonded supramolecular crosslinked

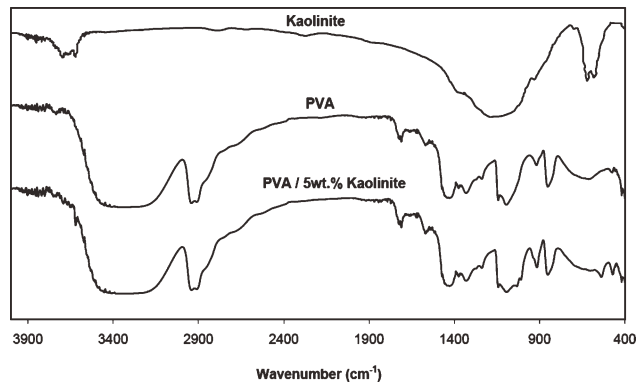

Figure 4 FTIR spectra of kaolinite powder, pure PVA hydrogel and nanocomposite hydrogel containing 5 wt % kaolinite.

structure of nanocomposite hydrogels. The increased gel fraction values of nanocomposite hydrogels are in consistence with the FTIR results and SEM observations.

DSC

Figure 6 shows the thermograms obtained by DSC measurements at the temperature range from −50 to 150°C for dried PVA hydrogel and nanocomposite hydrogels with 10 and 15 wt % kaolinite. The presence of kaolinite in the PVA hydrogel causes the shifting of glass transition temperature (T_g) to higher temperatures. Furthermore, T_g increases with increasing the kaolinite loading level in the nanocomposite hydrogels. This apparent increase may be attributed to the restricted mobility of the subchains in the polymeric network due to the presence of kaolinite layers and interaction creation among them, which were previously confirmed by the FTIR and gel fraction methods. The apparent endothermic peaks around 0°C could be attributed to the melting and solid–liquid phase transition of the remaining water molecules inside the dried hydrogels.

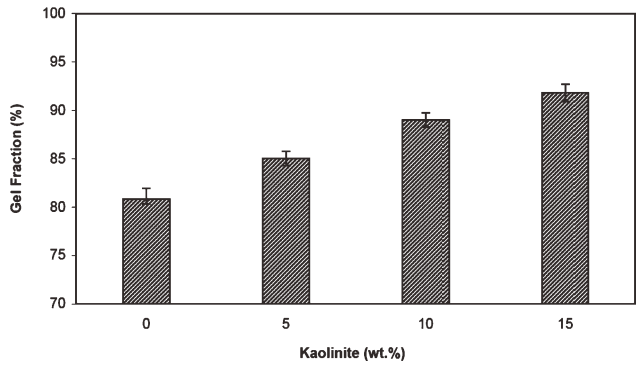

Figure 5 The effect of kaolinite loading level on the gel fraction values of hydrogels.

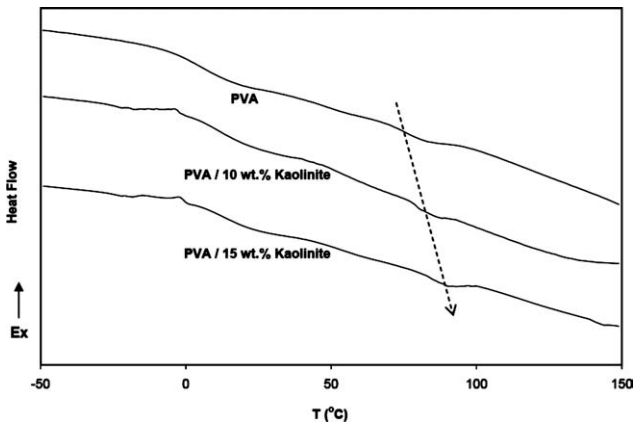

Figure 6 DSC thermograms of pure PVA hydrogel and nanocomposite hydrogels with 10 and 15 wt % kaolinite.

DMTA

The DMTA curves of hydrogels are shown in Figure 7 as storage modulus (E') and tan δ values versus temperature at a fixed frequency. It can be observed that all hydrogels exhibit same trends for both storage modulus and tan δ curves. At lower temperatures (<0°C), the storage modulus of each hydrogel is at high magnitude and decreases gradually with increase in temperature. At this temperature range, water molecules in hydrogels are in frozen state and thus hydrogels have very rigid nature with a high storage modulus. As the temperature reaches around 0°C, the storage modulus declines sharply by several orders of magnitude and a peak is created in tan δ curve due to solid–liquid phase transition of water molecules inside the hydrogel. After the phase transition, the storage modulus is decreased slightly with increase in temperature. Storage moduli of all nanocomposite hydrogels are higher than that of the pure PVA hydrogel over the whole temperature range. Further, the storage modulus increases by increasing the kaolinite content in nanocomposite hydrogels. For instance, the storage modulus of nanocomposite hydrogel containing 5 wt % of kaolinite in the regions below and above 0°C are on average 125 and 14% higher than of the pure PVA hydrogel, respectively. Although, 275 and 40% increases for storage modulus in the regions below and above 0°C are observed by adding 15 wt % of kaolinite to PVA hydrogel, respectively. The higher moduli of nanocomposite hydrogels shows the reinforcing effect of kaolinite in PVA matrix which could be attributed to the higher gel fraction values of nanocomposite hydrogels.

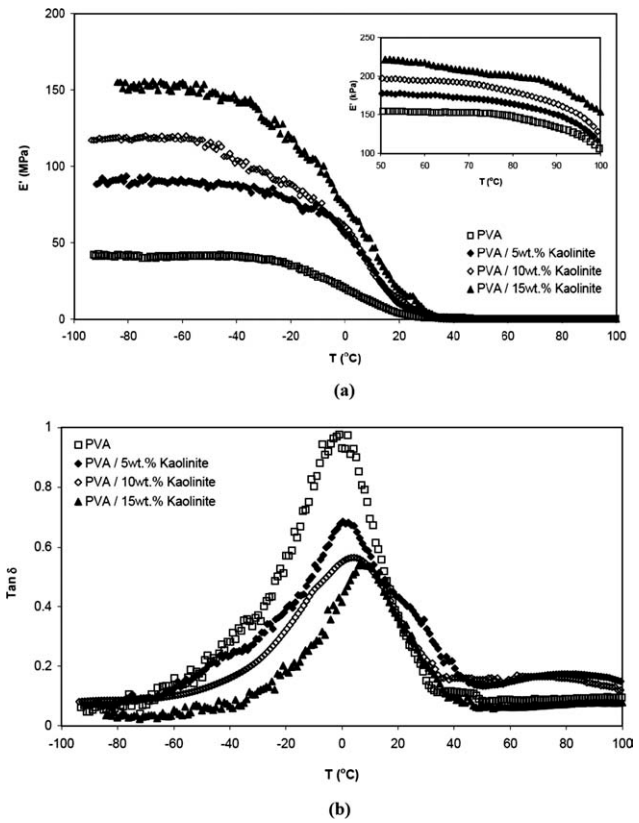

Figure 7 DMTA curves of hydrogels: (a) storage modulus and (b) tan δ.

Hardness

The relation between the Shore A hardness and kaolinite content in nanocomposite hydrogels has been shown in Figure 8. It can be seen that the hardness is directly depended to the quantity of kaolinite added to the nanocomposite hydrogel. The hardness of PVA hydrogel could increase by 34.2% by incorporating 15 wt % of kaolinite. The increase in hardness might be attributed to the increase in crystallinity and gel fraction of the hydrogel network. Improved hardness is in concordance with the increased mechanical properties of nanocomposite hydrogels obtained from DMTA results.

Swelling kinetics

The swelling ratio curves versus time showing the swelling kinetics of hydrogels in DDW are

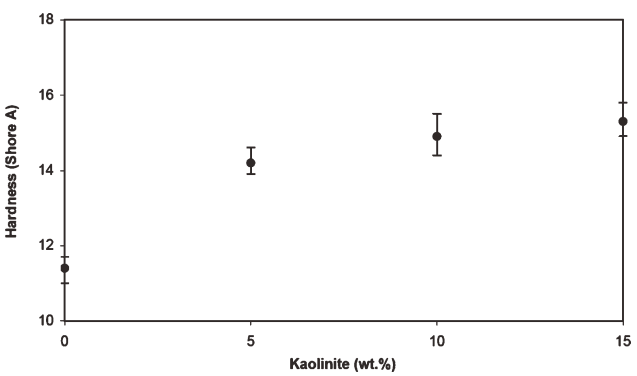

Figure 8 Shore A hardness of hydrogels.

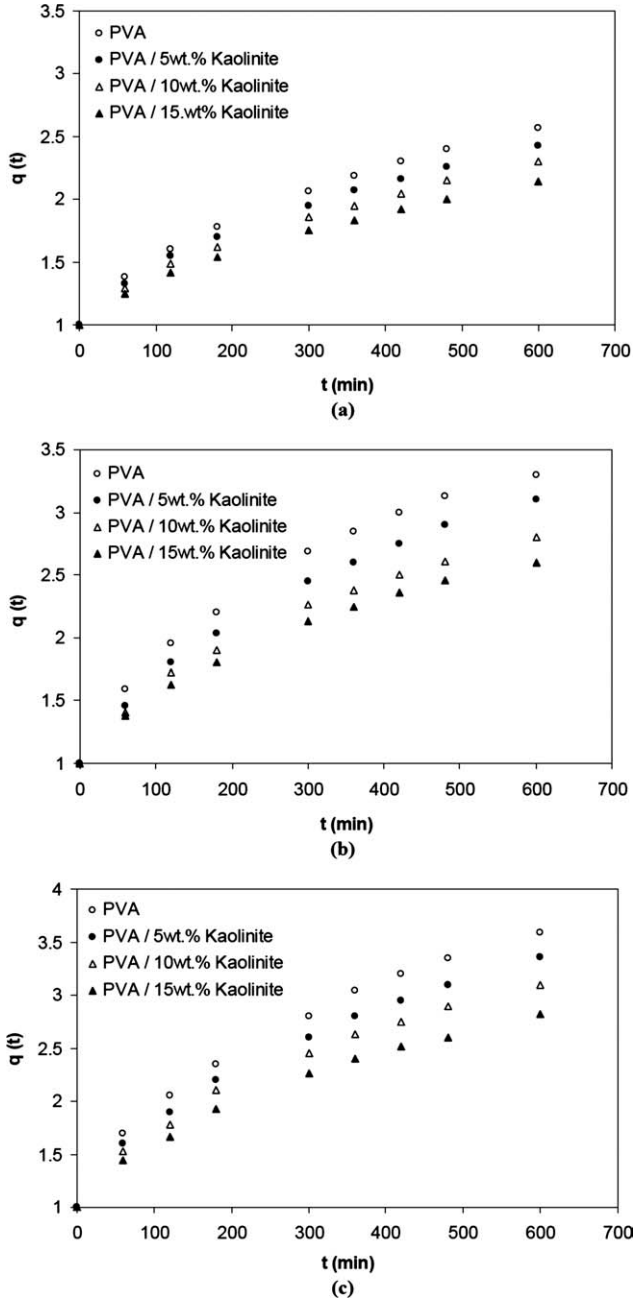

Figure 9 Swelling ratio curves of hydrogels versus time at swelling temperature of (a) 20, (b) 37, and (c) 55°C.

demonstrated in Figure 9 at different swelling temperatures, i.e., 20, 37, and 55°C. Swelling ratios of all hydrogel samples at all the swelling temperatures are increased with prolonged time. It is also observed that an increase in kaolinite content causes a decrease of the swelling ratio of nanocomposite hydrogels. The direct reason for the lower swelling ratios of nanocomposite hydrogels is the addition of kaolinite to PVA hydrogel network, which led to increase in the gel fraction values and as a result, the overall decrease on the swelling capability of the hydrogels.

The results also indicate that nanocomposite hydrogels exhibit slower swelling process with prolonged duration compared with the pure PVA hydrogel. This could be attributed to the slower and more prolonged mass transfer process of the swelling agent (water molecules) in nanocomposite hydrogel network. This might be attributed to the smaller pore size and less available free volume for diffusion of swelling agent molecules inside the nanocomposite hydrogels. Furthermore, the layers of clay inside the nanocomposite hydrogel network act as physical barrier against molecules transport due

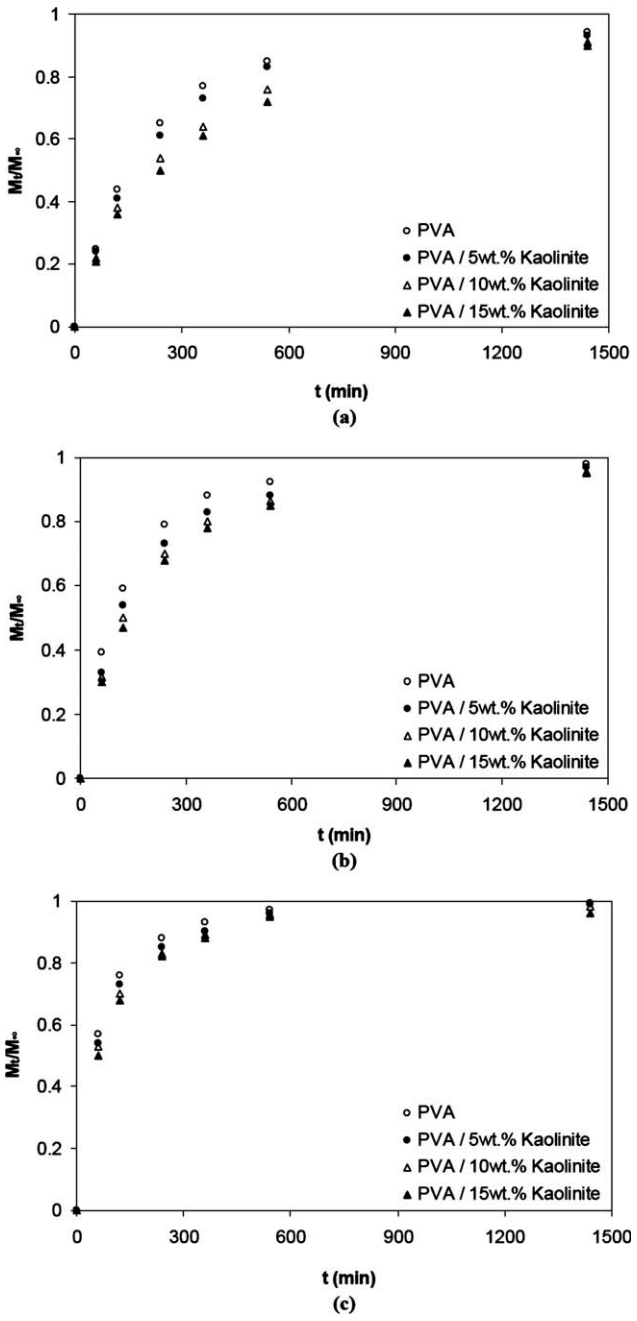

Figure 10 Dehydration kinetics curves of hydrogels at temperature of (a) 20, (b) 37, and (c) 55°C.

to creating more tortuous paths, which offers an additional controlling step against mass transfer as well as swelling process. Thus, it can be remarked that the nanocomposite hydrogels reach to a specific level of swelling at a much longer time and show slower swelling kinetics compared to clay-free hydrogel sample.

Figure 9 also show that the swelling ratios of all hydrogels are affected by the swelling medium temperature. At higher temperatures, the hydrogels can uptake more water and pose higher swelling ratios. This is attributed to the decrease of the Flory polymer–solvent interaction parameter as well as increase of the polymer chains flexibility by increasing the temperature.

Kinetics and mechanism of dehydration

Dehydration kinetics of the hydrogels was determined by plotting M_t/M_∞ values versus time for each sample at different drying temperatures. Figure 10 shows the time-dependent dehydration curves of hydrogels at 20, 37, and 55°C. Nearly identical patterns are observed for the dehydration curves of all samples at different constant temperatures. Dehydration curves of the nanocomposite hydrogels at any dehydration temperature show that the dehydration ability of hydrogel is decreased by increasing of the kaolinite loading level. In other words, nanocomposite hydrogels containing higher level of kaolinite exhibit longer dehydration duration. Like the swelling results, this could be attributed to the higher gel fraction value and more entangled structure of the nanocomposite hydrogels containing higher level of kaolinite. It can also be seen that the dehydration rates of hydrogels rise by increasing of drying temperature. This is due to the increase of diffusion coefficient of water in hydrogel matrix and its faster shrinkage process due to easier relaxation of polymer chains at higher temperatures.

To determine the mass transfer mechanism during the dehydration process of hydrogels, the following power law equation, describing the time-dependent dehydration process, was used:

$$\frac{M_t}{M_\infty} = Kt^n \tag{4}$$

where K is the dehydration characteristic constant and n is the characteristic exponent of the mode transport of the water from hydrogel. According to the classification of the diffusion mechanism, $n = 0.5$ and $0.5 < n < 1$ indicate the Fickian and non-Fickian (anomalous) diffusion mechanisms, respectively. The values of n and K were calculated for each hydrogel from the slope and intercept of the plot of $\log(M_t/M_\infty)$ against $\log(t)$ for $M_t/M_\infty < 0.6$, respectively. A good linear relation was observed between $\log(M_t/M_\infty)$ and $\log(t)$ for each hydrogel. The values of constants n and K for all hydrogels are shown in Table II. According to the calculated values for constant n, the dehydration mechanism of all hydrogels is a Fickian at 55°C. In addition, the mechanism of transport for hydrogels in other dehydration temperatures (i.e., 20 and 37°C) is considered as non-Fickian.

TABLE II
Dehydration Characteristics (Constants n and K) of Hydrogels

Kaolinite wt % (temperature)	n	K
0 (20°C)	0.6278	0.0202
5 (20°C)	0.6215	0.0197
10 (20°C)	0.5924	0.0205
15 (20°C)	0.5860	0.0201
0 (37°C)	0.4567	0.0627
5 (37°C)	0.6215	0.0197
10 (37°C)	0.5226	0.0387
15 (37°C)	0.5393	0.0341
0 (55°C)	0.2712	0.1955
5 (55°C)	0.2821	0.1777
10 (55°C)	0.2885	0.1680
15 (55°C)	0.3153	0.1427

CONCLUSIONS

In this work, nanocomposite hydrogels on the basis of PVA and kaolinite were prepared via the repeatedly freezing–thawing method. XRD and TEM results showed an intercalated morphology for prepared nanocomposite hydrogels. The FTIR and gel fraction tests revealed the interaction developments among the hydroxyl groups of PVA chains and kaolinite layers during the freezing–thawing process and showed the creation of supramolecular crosslinked structure of nanocomposite hydrogels. Thermal and mechanical experiments (i.e., DSC, DMTA, and hardness) demonstrated the reinforcing effect of kaolinite in PVA hydrogel matrix and exhibited of some increase in glass transition temperature of PVA hydrogel in presence of kaolinite. It was also observed that an increase of kaolinite content causes a decrease in the swelling ratio as well as in the dehydration rate of nanocomposite hydrogels. On the other hand, direct dependences of the swelling ratio and dehydration rate to temperature were observed for all nanocomposite hydrogels. In general, it seems that the freeze-thawed PVA nanocomposite hydrogels loaded with kaolinite are good candidate to be used as applicable material, with improved physical and mechanical properties, in practical applications. They could be recognized as promising materials for biomedical applications, due to absence of any additional toxic crosslinker or modifier agents for modification of kaolinite, such as DMSO.

References

1. Kobayashi, M.; Toguchida, J.; Oka, M. J Biomed Mater Res Appl Biomater 2001, 58, 344.
2. Chen, D. H.; Leu, J. C.; Huang, T. C. J Chem Technol Biotechnol 1994, 61, 351.
3. Hyon, S. H.; Cha, W. I.; Ikada, Y.; Kita, M.; Ogura, Y.; Honda, Y. J Biomater Sci Polym Ed 1994, 5, 397.
4. More, S. M.; Kulkarni, R. V.; Sa, B.; Kayane, N. V. J Appl Polym Sci 2010, 116, 1732.
5. Kenawy, E. R.; El-Newehy, M. H.; Al-Deyab, S. S. J Saudi Chem Soc 2010, 14, 237.
6. Sirousazar, M.; Kokabi, M.; Yari, M. Iran J Pharm Sci 2008, 4, 51.
7. Sirousazar, M.; Yari, M. Chin J Polym Sci 2010, 28, 573.
8. Gupta, A.; Kumar, R.; Upadhyay, N. K.; Surekha, P.; Roy, P. K. J Appl Polym Sci 2009, 111, 1400.
9. Bolto, B.; Tran, T.; Hoang, M.; Xie, Z. Prog Polym Sci 2009, 34, 969.
10. Liu, Y.; Vrana, N. E.; Cahill, P. A.; McGuinness, G. B. J Biomed Mater Res B 2009, 90, 492.
11. Peppas, N. A. Makromol Chem 1975, 176, 3433.
12. Hassan C. M.; Peppas, N. A. Adv Polym Sci 2000, 153, 37.
13. Haraguchi, K.; Takehisa, T. Adv Mater 2002, 14, 1120.
14. Schexnailder, P.; Schmidt, G. Colloid Polym Sci 2009, 287, 1.
15. Gant, R. M.; Hou, Y.; Grunlan, M. A.; Cote, G. L. J Biomed Mater Res A 2009, 90, 695.
16. Zolfaghari, R.; Katbab, A. A.; Nabavizadeh, J.; Tabasi, R. Y.; Nejad, M. H. J Appl Polym Sci 2006, 100, 2096.
17. Wang, M.; Li, Y.; Wu, J.; Xu, F.; Zuo, Y.; Jansen, J. A. J Biomed Mater Res A 2008, 85, 418.
18. Satarkar, N. S.; Hilt, J. Z. Acta Biomater 2008, 4, 11.
19. Liu, K. H.; Liu, T. Y.; Chen, S. Y.; Liu, D. M. Acta Biomater 2008, 4, 1038.
20. Kokabi, M.; Sirousazar, M.; Hassan, Z. M. Eur Polym J 2007, 43, 773.
21. Sirousazar, M.; Kokabi, M.; Hassan, Z. M. J Biomater Sci Polym Ed 2011, 22, 1023.
22. Abdurrahmanoglu, S.; Can, V.; Okay, O. J Appl Polym Sci 2008, 109, 3714.
23. Sirousazar, M.; Kokabi, M.; Hassan, Z. M.; Bahramian, A. R. Sci Iran Trans F Nanotech, DOI: 10.1016/j.scient.2011.06.002.
24. Sirousazar, M.; Kokabi, M.; Hassan, Z. M. J Appl Polym Sci DOI: 10.1002/app.34437.
25. Lee, W. F.; Lee, S. C. J Appl Polym Sci 2006, 100, 500.
26. Zhang, X.; Xu, Z. Mater Lett 2007, 61, 1478.
27. Stellano, M.; Turturro, A.; Riani, P.; Montanari, T.; Finocchio, E.; Ramis, G. Busca, G. Appl Clay Sci 2010, 48, 446.
28. Wang, Y. L.; Lee, B. S.; Chang, K. C.; Chiu, H. C.; Lin, F. H.; Lin, C. P. Compos Sci Technol 2007, 67, 3409.
29. Bahramian, A. R.; Kokabi, M.; Famili, M. H. N.; Beheshty, M. H. J Hazard Mater 2008, 150, 136.
30. Villanueva, M. P.; Cabedo, L.; Lagaron, J. M.; Gimenez, E. J Appl Polym Sci 2010, 115, 1325.
31. Kabiri, K.; Zohuriaan-Mehr, M. J. Polym Adv Technol 2003, 14, 438.
32. Pourjavadi, A.; Ghasemzadeh, H.; Soleyman, R. J Appl Polym Sci 2007, 105, 2631.
33. Liang, R.; Liu, M. J Appl Polym Sci 2007, 106, 3007.
34. Pourjavadi, A.; Ayyari, M.; Amini-Fazl, M. S. Eur Polym J 2008, 44, 1209.
35. Zhao, X.; Wang, B.; Li, J. J Appl Polym Sci 2008, 108, 2833.
36. Kabiri, K.; Mirzadeh, H.; Zohuriaan-Mehr, M. J. J Appl Polym Sci 2010, 116, 2548.